Eidgenössische Technische Hochschule Zürich

Ecole polytechnique fédérale de Zurich
Politecnico federale di Zurigo
Swiss Federal Institute of Technology Zurich

Entropy stable numerical schemes for two-fluid MHD equations

H. Kumar and S. Mishra

Research Report No. 2011-22
April 2011

Seminar für Angewandte Mathematik
Eidgenössische Technische Hochschule
CH-8092 Zürich
Switzerland

ENTROPY STABLE NUMERICAL SCHEMES FOR TWO-FLUID MHD EQUATIONS

HARISH KUMAR AND SIDDHARTHA MISHRA

Abstract. Two-fluid ideal magnetohydrodynamics (MHD) equations are a generalized form of the ideal MHD equations in which electrons and ions are considered as separate species. The design of efficient numerical schemes for the these equations is complicated on account of their non-linear nature and the presence of stiff source terms, especially for high charge to mass ratios. In this article, we design entropy stable finite difference schemes for the two-fluid equations by combining entropy conservative fluxes and suitable numerical diffusion operators. Furthermore, to overcome the time step restrictions imposed by the stiff source terms, we devise time-stepping routines based on implicit-explicit (IMEX)-Runge Kutta (RK) schemes. The special structure of the two-fluid MHD equations is exploited by us to design IMEX schemes in which only local (in each cell) linear equations need to be solved at each time step. Benchmark numerical experiments are presented to illustrate the robustness and accuracy of these schemes.

1. Introduction

An ensemble of plasma consists of ions, electrons and neutral particles. These particles interact through both short range (e.g. collisions) and long range (e.g. electromagnetic) forces. Plasmas are increasingly used in spacecraft propulsion, controlled nuclear fusion and in circuit breakers in the electrical power industry.

Under the assumption of *quasi-neutrality* (i.e. charge density difference between ions and electrons is neglected), the flow of plasmas is modeled by the ideal MHD equations (see [8]). Although, the ideal MHD equations have been successfully employed in modeling and simulating plasma flows, this model is derived by ignoring the Hall effect and treating plasma flows as *single* fluid flows. These effects are very important for many applications, e.g. space plasmas, Hall current thrusters, field reversal configurations for magnetic plasma confinement and for fast magnetic reconnection.

In this article, we consider the more general ideal two-fluid model (see [15],[13],[9]) for collisionless plasmas. In the ideal two-fluid equations, electrons and ions are treated as different fluids by allowing them to posses different velocities and temperatures. Assuming *local thermodynamical equilibrium*, we write the two-fluid equations as a system of balance laws (see [9]):

$$\partial_t \mathbf{u} + \text{div } \mathbf{f}(\mathbf{u}) = \mathbf{s}(\mathbf{u}), \quad (\mathbf{x}, t) \in \mathbb{R}^3 \times (0, \infty). \tag{1.1}$$

Here, $\mathbf{u} = \mathbf{u}(x, y, z, t)$ is the vector of non-dimensional conservative variables,

$$\mathbf{u} = \{\rho_i, \rho_i \mathbf{v}_i, E_i, \rho_e, \rho_e \mathbf{v}_e, E_e, \mathbf{B}, \mathbf{E}, \phi, \psi\}^\top. \tag{1.2}$$

Here, the subscripts $\{i, e\}$ refer to the ion and electron species respectively, $\rho_{\{i,e\}}$ are the densities, $\mathbf{v}_{\{i,e\}} = (v^x_{\{i,e\}}, v^y_{\{i,e\}}, v^z_{\{i,e\}})$ are the velocities, $E_{\{i,e\}}$ are the total energies, $\mathbf{B} = (B^x, B^y, B^z)$ is the magnetic field, $\mathbf{E} = (E^x, E^y, E^z)$ is the electric field and ϕ, ψ are the potentials. The flux

vector $\mathbf{f} = (\mathbf{f}^x, \mathbf{f}^y, \mathbf{f}^z)$ can be written as,

$$\mathbf{f}(\mathbf{u}) = \left\{ \begin{array}{c} \mathbf{f}_i(\mathbf{u}_i) \\ \mathbf{f}_e(\mathbf{u}_e) \\ \mathbf{f}_m(\mathbf{u}_m) \end{array} \right\}, \quad \text{where} \quad \mathbf{f}_\alpha(\mathbf{u}_\alpha) = \left\{ \begin{array}{c} \rho_\alpha \mathbf{v}_\alpha \\ \rho_i \mathbf{v}_\alpha \mathbf{v}_\alpha^\top + p_\alpha \mathbf{I} \\ (E_\alpha + p_\alpha)\mathbf{v}_\alpha \end{array} \right\}, \tag{1.3}$$

with $\alpha \in \{i, e\}$, and

$$\mathbf{f}_m(\mathbf{u}_m) = \left\{ \begin{array}{c} \mathcal{T}(\mathbf{E}) + \kappa\psi \mathbf{I} \\ -\hat{c}^2 \mathcal{T}(\mathbf{B}) + \xi \hat{c}^2 \phi \mathbf{I} \\ \xi \mathbf{E} \\ \kappa \hat{c}^2 \mathbf{B} \end{array} \right\}, \text{ where } \mathcal{T}(\mathbf{K}) = \left[\begin{array}{ccc} 0 & K^z & -K^y \\ -K^z & 0 & K^x \\ K^y & -K^x & 0 \end{array} \right], \tag{1.4}$$

for any vector $\mathbf{K} = (K^x, K^y, K^z)$. Here $\mathbf{u}_\alpha = \{\rho_\alpha, \rho_\alpha \mathbf{v}_\alpha, E_\alpha\}^\top$, $\alpha \in \{i, e\}$, $\mathbf{u}_m = \{\mathbf{B}, \mathbf{E}, \phi, \psi\}^\top$, $p_{\{i,e\}}$ are the pressures, ξ, κ are penalizing speeds (see [14]) and $\hat{c} = c/v_i^T$ is the normalized speed of light. Also, v_i^T is the reference thermal velocity of ion. Writing the flux in component form (see (1.3),(1.4)), we observe that the first two components of the flux, $\mathbf{f}_\alpha(\mathbf{u}_\alpha)$, $\alpha \in \{i, e\}$, are the nonlinear ion and electron Euler fluxes and the third component is the linear Maxwell flux. So, the homogenous part of (1.1) is hyperbolic.

The source term $\mathbf{s}$ is given by,

$$\mathbf{s}(\mathbf{u}) = \left\{ \begin{array}{c} 0 \\ \frac{1}{\hat{r}_g} \rho_i (\mathbf{E} + \mathbf{v}_i \times \mathbf{B}) \\ 0 \\ -\frac{\lambda_m}{\hat{r}_g} \rho_e (\mathbf{E} + \mathbf{v}_e \times \mathbf{B}) \\ -\frac{\lambda_m}{\hat{r}_g} \rho_e (\mathbf{E} \cdot \mathbf{v}_e) \\ \mathbf{0} \\ -\frac{1}{\hat{\lambda}_d^2 \hat{r}_g} (r_i \rho_i \mathbf{v}_i + r_e \rho_e \mathbf{v}_e) \\ -\frac{\xi}{\hat{\lambda}_d^2 \hat{r}_g} (r_i \rho_i + r_e \rho_e) \\ 0 \end{array} \right\}, \tag{1.5}$$

with the charge to mass ratios $r_\alpha = q_\alpha/m_\alpha$, $\alpha \in \{i, e\}$ and the ion-electron mass ratio $\lambda_m = m_i/m_e$. Two physically significant parameters appear in the source term namely, the normalized Larmor radius $\hat{r}_g = \frac{r_g}{x_0} = \frac{m_i v_i^T}{q_i B_0 x_0}$ and the ion Debye length (normalized with respect to the Larmor radius) $\hat{\lambda}_d = \lambda_d / r_g = \sqrt{\varepsilon_0 v_i^{T^2} / n_0 q_i} / r_g$. Here, B_0 is the reference magnetic field, ε_0 is the permittivity of free space and x_0 is the reference length. The ion mass m_i and ion charge q_i are assumed to be 1. In addition, we assume that both the ion and the electron satisfies the ideal gas law:

$$E_\alpha = \frac{p_\alpha}{\gamma - 1} + \frac{1}{2} \rho_\alpha |\mathbf{v}_\alpha|^2, \quad \alpha \in \{i, e\}, \tag{1.6}$$

with gas constant $\gamma = 5/3$. In the above equations, we use the perfectly hyperbolic form of the Maxwell equation (see [14]), which represent the evolution of magnetic field $\mathbf{B}$ and electric field $\mathbf{E}$.

The design of numerical schemes for systems of balance laws has undergone rapid development in the last two decades, see [12] for a detailed description of efficient schemes. The standard paradigm involves the use of finite volume (conservative finite difference) schemes in which the solution is evolved in terms of (approximate) solutions of Riemann problems at cell interfaces. Higher order accuracy in space is obtained by non-oscillatory interpolation procedures of the TVD, ENO and WENO types. An alternative is to use the Discontinuous Galerkin

(DG) approach. High-order temporal accuracy results from strong stability preserving (SSP) Runge-Kutta (RK) methods. Source terms are included by using operator splitting approaches.

Although the two-fluid equations are a system of balance laws, standard discretization techniques may fail to provide a robust approximation. Two major difficulties are present in the numerical analysis of the two-fluid equations: 1) the design of suitable numerical fluxes and 2) treatment of the source term that becomes increasingly stiffer as more realistic charge to mass ratios are considered.

Given the above challenges, very few robust numerical schemes exist for the two-fluid equations. In [15], the authors derive a Roe-type Riemann solver. Time updates are performed by treating the stiff source term implicitly and the flux terms explicitly. The resulting non-linear equations are solved using Newton iterations. This method might be diffusive and may require many iterations for each time step. In [9], the authors propose a wave propagation method (see [12]) for the spatial discretization. For time updates, a second -order operator splitting approach is used. A similar approach is taken in [13, 11], where spatial discretization is based on discontinuous Galerkin (DG) methods and time update is based on SSP-RK methods. Both of these approaches are easy to implement but can be computationally expensive, especially for realistic charge to mass ratios.

Given the state of the art, we propose numerical schemes for the two-fluid equations with the following *novel* features:

- First, we design entropy stable, conservative, finite difference discretization of the flux term in the two fluid equations. The basis of our design is to ensure entropy stability as the two fluid equations satisfy an entropy inequality at the continuous level. We use the approach of [17] by constructing entropy conservative fluxes and suitable numerical diffusion operators to ensure entropy stability. Second-order entropy stable schemes are constructed following the framework of a recent paper [6].
- We discretize the source term in the two-fluid equations by an IMEX approach: the flux terms are discretized explicitly whereas the source term is discretized implicitly. The main feature of our schemes is their ability to use the special structure of the two-fluid equations that allows us to design IMEX schemes requiring the solution of only local (in each cell) linear equations at every time step. This is in contrast to the schemes proposed in [15] that required the solution of non-linear iterations. The local equations that result from our approach can be solved exactly making our schemes computationally inexpensive.

The rest of this article is organized as follows: In the following Section 2, we obtain an entropy estimate for the ideal two-fluid eqns. (1.1). This result at the continuous level is then used to design an entropy stable finite difference scheme in Section 3. In Section 4, we present IMEX-RK schemes for the temporal discretization. The resulting, algebraic system of equations is then solved exactly. In Section 5, we simulate the nonlinear soliton propagation in the two-fluid plasma and a stiff Riemann problem to demonstrate the robustness and efficiency of these schemes.

2. Analysis of Continuous Problem

It is well known that solutions of (1.1) consists discontinuities, even for smooth initial data. Hence, we need to consider the solutions of (1.1) in the weak sense. However, uniqueness of the solutions is still not guaranteed and we need to supplement (1.1) with additional admissibility criteria to obtain a physically meaningful solution. This gives rise to concept of entropy. The standard thermodynamic entropies for ion and electron Euler flows are,

$$e_\alpha = -\frac{\rho_\alpha s_\alpha}{\gamma - 1} \quad \text{with} \;\; s_\alpha = \log(p_\alpha) - \gamma \log(\rho_\alpha), \quad \alpha \in \{i, e\}. \tag{2.1}$$

For the electromagnetic part we consider the *quadratic* entropy i.e electromagnetic energy,

$$e_m(\mathbf{u}_m) = \frac{|\mathbf{B}|^2 + \phi^2}{2} + \frac{|\mathbf{E}|^2 + \psi^2}{2\hat{c}^2}. \tag{2.2}$$

We obtain the following entropy estimate,

Theorem 2.1. *Let* $\mathbf{u} = \{\rho_i, \rho_i \mathbf{v}_i, E_i, \rho_e, \rho_e \mathbf{v}_e, E_e, \mathbf{B}, \mathbf{E}, \phi, \psi\}^\top$ *be a weak solution of the two-fluid Eqns.* (1.1) *on* $\mathbb{R}^3 \times (0, \infty)$. *Furthermore, assume that there exists constants* $\rho_\alpha^{\min}, \rho_\alpha^{\max}$ *and* $p_\alpha^{\min}$ *such that,*

$$\rho_\alpha^{\min} \leq \rho_\alpha \leq \rho_\alpha^{\max}, \quad p_\alpha \geq p_\alpha^{\min}, \quad \alpha \in \{i, e\},$$

then

$$\frac{d}{dt}\int_{\mathbb{R}^3} (e_i + e_e + e_m)\, dx\, dy\, dz \leq C_1 \int_{\mathbb{R}^3} (e_i + e_e + e_m)\, dx\, dy\, dz + C_2, \tag{2.3}$$

with constant C_1 *and* C_2 *depending only on* $\rho_\alpha^{\min}, \rho_\alpha^{\max}$, *and* $p_\alpha^{\min}$.

Proof. Let us first consider the fluid part of the equations. The entropy fluxes corresponding to the flow entropies (2.1) are,

$$\mathbf{q}_\alpha = -\frac{\rho_\alpha s_\alpha \mathbf{v}_\alpha}{\gamma - 1} = \mathbf{v}_\alpha e_\alpha, \quad \alpha \in \{i, e\}. \tag{2.4}$$

Assuming that $\mathbf{u}$ is a smooth solution of (1.1), the densities ρ_α and the pressures p_α, satisfy,

$$\partial_t \rho_\alpha + \mathbf{v}_\alpha \cdot \nabla \rho_\alpha = 0,$$
$$\partial_t p_\alpha + \gamma p_\alpha \nabla \cdot \mathbf{v}_\alpha + \mathbf{v}_\alpha \cdot \nabla p_\alpha = 0.$$

Using the expression for s_α, we get

$$\partial_t s_\alpha + \mathbf{v}_\alpha \cdot \nabla s_\alpha = 0.$$

Combining this with density advection we get *entropy conservation*, i.e.

$$\partial_t e_\alpha + \nabla \cdot \mathbf{q}_\alpha = 0. \tag{2.5}$$

Observe that (2.5) implies that the source term does not effect the evolution of fluid entropies. For weak solutions, (2.5) reduces to *entropy inequality*,

$$\partial_t e_\alpha + \nabla \cdot \mathbf{q}_\alpha \leq 0. \tag{2.6}$$

Integrating over $\mathbb{R}^3$ and adding,

$$\frac{d}{dt}\int_{\mathbb{R}^3} (e_i + e_e) dx\, dy\, dz \leq 0. \tag{2.7}$$

For controlling the electromagnetic energy, we use the following inequality,

$$\int_{\mathbb{R}^3} \left(\rho_\alpha^2 + |\rho_\alpha \mathbf{v}_\alpha|^2 + E_\alpha^2\right)\ dx\, dy\, dz \leq C \int_{\mathbb{R}^3} e_\alpha dx\, dy\, dz + \overline{C}, \tag{2.8}$$

for some constants $C, \overline{C}$.The proof of (2.8) is a simple consequence of the positivity of density and pressure and the use of the relative entropy method of Dafermos [5]. We multiply (1.1) with the vector,

$$\left\{\mathbf{0}_{10}, \mathbf{B}, \frac{\mathbf{E}}{\hat{c}^2}, \phi, \frac{\psi}{\hat{c}^2}\right\}^\top$$

and note that flux terms are still in divergence form. Integrating over the whole space and using Cauchy's inequality on the right hand side, we get,

$$\frac{d}{dt}\int_{\mathbb{R}^3} e_m dx\, dy\, dz \leq C_3 \left(\int_{\mathbb{R}^3} e_m dx\, dy\, dz + \int_{\mathbb{R}^3} (e_i + e_e) dx\, dy\, dz\right) + C_4. \tag{2.9}$$

Combining it with (3.22) we obtain (2.3). □

Remark 2.2. Note that above proof of the theorem also give a bound on the fluid energy of the system.

3. Semi-Discrete Schemes

In the last section, we showed that solutions of the two-fluid equations satisfy the entropy estimate (2.3). In this section, we will design (semi-discrete) numerical schemes for the two-fluid equations that satisfy a discrete version of the entropy estimate.

For simplicity, we consider two-fluid eqns. (1.1) in two dimensions, i.e.,

$$\partial_t \mathbf{u} + \partial_x \mathbf{f}^x(\mathbf{u}) + \partial_y \mathbf{f}^y(\mathbf{u}) = \mathbf{s}(\mathbf{u}). \tag{3.1}$$

We discretize the two dimensional rectangular domain $D = (x_a, x_b) \times (y_a, y_b)$ uniformly with mesh size $(\Delta x, \Delta y)$. We define $x_i = x_a + i\Delta x$ and $y_j = y_a + j\Delta y$, $0 \le i \le N_x$, $0 \le j \le N_y$, such that $x_b = x_a + N_x\Delta x$ and $y_b = y_a + N_y\Delta x$. The domain is then divided into cells $I_{ij} = [x_{i-1/2}, x_{i+1/2}] \times [y_{j-1/2}, y_{j+1/2}]$ with $x_{i+1/2} = \frac{x_i + x_{i+1}}{2}$ and $y_{j+1/2} = \frac{y_j + y_{j+1}}{2}$. A standard semi-discrete finite difference scheme for the eqn. (3.1) can be written as,

$$\frac{d\mathbf{U}_{i,j}}{dt} + \frac{1}{\Delta x}\left(\mathbf{F}^x_{i+1/2,j} - \mathbf{F}^x_{i-1/2,j}\right) + \frac{1}{\Delta y}\left(\mathbf{F}^y_{i,j+1/2} - \mathbf{F}^y_{i,j-1/2}\right) = \mathbf{s}(\mathbf{U}_{i,j}). \tag{3.2}$$

Here, $\mathbf{F}^x_{i+1/2,j}$ and $\mathbf{F}^y_{i,j+1/2}$ are the numerical fluxes consistent with $\mathbf{f}^x$ and $\mathbf{f}^y$ respectively. We introduce the *entropy variables* $\mathbf{V}$ and *entropy potential* χ^k which corresponds to the entropy $e = \{e_i, e_e, e_m\}^\top$

$$\mathbf{V} = \begin{Bmatrix} \mathbf{V}_i \\ \mathbf{V}_e \\ \mathbf{V}_m \end{Bmatrix} = \begin{Bmatrix} \partial_{\mathbf{u}_i} e_i(\mathbf{u}_i) \\ \partial_{\mathbf{u}_e} e_e(\mathbf{u}_e) \\ \partial_{\mathbf{u}_m} e_m(\mathbf{u}_m) \end{Bmatrix}, \qquad \chi^k = \begin{Bmatrix} \chi^k_i \\ \chi^k_e \\ \chi^k_m \end{Bmatrix} = \begin{Bmatrix} \mathbf{V}_i^\top \mathbf{f}^k_i - \mathbf{q}^k_i \\ \mathbf{V}_e^\top \mathbf{f}^k_e - \mathbf{q}^k_e \\ \mathbf{V}_m^\top \mathbf{f}^k_m - \mathbf{q}^k_m \end{Bmatrix}, \tag{3.3}$$

where $\mathbf{q}^k_m$ is the entropy flux for the Maxwell part corresponding to the entropy e_m and $k \in \{x, y\}$. We will follow the framework of Tadmor (see [17, 18]) for designing an entropy stable scheme for the two-fluid equations. The first step is to design an entropy conservative flux.

3.1. Entropy conservative flux.

We require the following notation:

$$[a]_{i+1/2,j} = a_{i+1,j} - a_{ij}, \quad \overline{a}_{i+1/2,j} = \frac{1}{2}(a_{i+1,j} + a_{i,j}),$$
$$[a]_{i,j+1/2} = a_{i,j+1} - a_{ij}, \quad \overline{a}_{i,j+1/2} = \frac{1}{2}(a_{i,j+1} + a_{i,j}).$$

Following [17], an entropy conservative flux $\hat{\mathbf{F}} = \{\hat{\mathbf{F}}^x, \hat{\mathbf{F}}^y\}$ is defined as a consistent flux that satisfies

$$[\mathbf{V}]^\top_{i+1/2,j} \hat{\mathbf{F}}^x_{i+1/2,j} = [\chi^x]_{i+1/2,j}, \qquad [\mathbf{V}]^\top_{i,j+1/2} \hat{\mathbf{F}}^y_{i,j+1/2} = [\chi^y]_{i,j+1/2}. \tag{3.4}$$

In general, the relation for conservative flux, (3.4) provides one equation for several unknowns. Hence, entropy conservative numerical flux is not unique. We will now describe entropy conservative numerical fluxes for the fluid part of the two-fluid equations.

In [10], Ismail and Roe have derived an expression for entropy conservative numerical fluxes for Euler equations of gas dynamics. As the fluid part of (1.1) consists of two independent Euler fluxes, we can use the expression derived in [10] for the entropy conservative numerical flux of

the Euler flows of ion and electron. We need to introduce parametric vectors $\mathbf{z}_\alpha,\ \ \alpha \in \{i, e\}$,

$$\mathbf{z}_\alpha = \begin{bmatrix} z_\alpha^1 \\ z_\alpha^2 \\ z_\alpha^3 \\ z_\alpha^4 \\ z_\alpha^5 \end{bmatrix} = \sqrt{\frac{\rho_\alpha}{p_\alpha}} \begin{bmatrix} 1 \\ v_\alpha^x \\ v_\alpha^y \\ v_\alpha^z \\ p_\alpha \end{bmatrix}, \qquad \alpha \in \{i, e\}. \tag{3.5}$$

Then the entropy conservative numerical flux in x-direction is given by $\hat{\mathbf{F}}^x_{\alpha,i+1/2,j} = [\hat{\mathbf{F}}^{x,1}_{\alpha,i+1/2,,j}, \hat{\mathbf{F}}^{x,2}_{\alpha,i+1/2,j}, \hat{\mathbf{F}}^{x,3}_{\alpha,i+1/2,j}, \hat{\mathbf{F}}^{x,4}_{\alpha,i+1/2,j}, \hat{\mathbf{F}}^{x,5}_{\alpha,i+1/2,j}]^\top$, with,

$$\begin{aligned}
\hat{\mathbf{F}}^{x,1}_{\alpha,i+1/2,j} &= \overline{z^2}_{\alpha,i+1/2,j} {z^5}^{\ln}_{\alpha i+1/2,j}, \\
\hat{\mathbf{F}}^{x,2}_{\alpha,i+1/2,j} &= m^5_{\alpha,i+1/2,j} + m^2_{\alpha,i+1/2,j} \hat{\mathbf{F}}^{x,1}_{\alpha,i+1/2,j}, \\
\hat{\mathbf{F}}^{x,3}_{\alpha,i+1/2,j} &= m^3_{\alpha,i+1/2,j} \hat{\mathbf{F}}^{x,1}_{\alpha,i+1/2,j}, \\
\hat{\mathbf{F}}^{x,4}_{\alpha,i+1/2,j} &= m^4_{\alpha,i+1/2,j} \hat{\mathbf{F}}^{x,1}_{\alpha,i+1/2,j}, \\
\hat{\mathbf{F}}^{x,5}_{\alpha,i+1/2,j} &= \frac{1}{2\overline{z^1}_{\alpha,i+1/2,j}} \left(\frac{\gamma+1}{\gamma-1} \frac{\hat{\mathbf{F}}^{x,1}_{\alpha,i+1/2,j}}{{z^1}^{\ln}_{\alpha,i+1/2,j}} + \overline{z^2}_{\alpha,i+1/2,j} \hat{\mathbf{F}}^{x,2}_{\alpha,i+1/2,j} \right. \\
&\quad \left. + \overline{z^3}_{\alpha,i+1/2} \hat{\mathbf{F}}^{x,3}_{\alpha,i+1/2,j} + \overline{z^4}_{\alpha,i+1/2,j} \hat{\mathbf{F}}^{x,4}_{\alpha,i+1/2,j} \right).
\end{aligned} \tag{3.6}$$

and entropy conservative numerical flux in y-direction is, $\hat{\mathbf{F}}^y_{\alpha,i,j+1/2} = [\hat{\mathbf{F}}^{y,1}_{\alpha,i,j+1/2}, \hat{\mathbf{F}}^{y,2}_{\alpha,i,j+1/2}, \hat{\mathbf{F}}^{y,3}_{\alpha,i,j+1/2}, \hat{\mathbf{F}}^{y,4}_{\alpha,i,j+1/2}, \hat{\mathbf{F}}^{y,5}_{\alpha,i,j+1/2}]^\top$, with,

$$\begin{aligned}
\hat{\mathbf{F}}^{y,1}_{\alpha,i,j+1/2} &= \overline{z^3}_{\alpha,i,j+1/2} {z^5}^{\ln}_{\alpha,i,j+1/2}, \\
\hat{\mathbf{F}}^{y,2}_{\alpha,i,j+1/2} &= m^2_{\alpha,i,j+1/2} \hat{\mathbf{F}}^{y,1}_{\alpha,i,j+1/2}, \\
\hat{\mathbf{F}}^{y,3}_{\alpha,i,j+1/2} &= m^3_{\alpha,i,j+1/2} + m^3_{\alpha,i,j+1/2} \hat{\mathbf{F}}^{y,1}_{\alpha,i,j+1/2}, \\
\hat{\mathbf{F}}^{y,4}_{\alpha,i,j+1/2} &= m^4_{\alpha,i,j+1/2} \hat{\mathbf{F}}^{y,1}_{\alpha,i,j+1/2}, \\
\hat{\mathbf{F}}^{y,5}_{\alpha,i,j+1/2} &= \frac{1}{2\overline{z^1}_{\alpha,i,j+1/2}} \left(\frac{\gamma+1}{\gamma-1} \frac{\hat{\mathbf{F}}^{y,1}_{\alpha,i,j+1/2}}{{z^1}^{\ln}_{\alpha,i,j+1/2}} + \overline{z^2}_{\alpha,i,j+1/2} \hat{\mathbf{F}}^{y,2}_{\alpha,i,j+1/2} \right. \\
&\quad \left. + \overline{z^3}_{\alpha,i,j+1/2} \hat{\mathbf{F}}^{y,3}_{\alpha,i,j+1/2} + \overline{z^4}_{\alpha,i,j+1/2} \hat{\mathbf{F}}^{y,4}_{\alpha,i,j+1/2} \right),
\end{aligned} \tag{3.7}$$

Here, $a^{ln}_{i+1/2,j}$ and $a^{ln}_{i,j+1/2}$ denotes the logarithmic means defined as,

$$a^{ln}_{i+1/2,j} = \frac{[a]_{i+1/2,j}}{[\log(a)]_{i+1/2,j}}, \qquad a^{ln}_{i,j+1/2} = \frac{[a]_{i,j+1/2}}{[\log(a)]_{i,j+1/2}},$$

and

$$m^r_{\alpha,i+1/2,j} = \frac{\overline{z^r}_{\alpha,i+1/2,j}}{\overline{z^1}_{\alpha,i+1/2,j}}, \qquad m^r_{\alpha,i,j+1/2} = \frac{\overline{z^r}_{\alpha,i,j+1/2}}{\overline{z^1}_{\alpha,i,j+1/2}}, \qquad \text{for} \qquad r \in \{2, 3, 4, 5\}.$$

Now we will consider the electromagnetic part. Note the Maxwell flux is linear. Then, it is easy to check that the entropy conservative numerical flux for the electromagnetic part is

$$\hat{\mathbf{F}}^x_{m,i+1/2,j} = \frac{1}{2}(\mathbf{f}^x(\mathbf{U}_{m,i,j}) + \mathbf{f}^x(\mathbf{U}_{m,i+1,j})), \quad \hat{\mathbf{F}}^y_{m,i,j+1/2} = \frac{1}{2}(\mathbf{f}^y(\mathbf{U}_{m,i,j}) + \mathbf{f}^y(\mathbf{U}_{m,i,j+1})). \tag{3.8}$$

Combining all the parts, the entropy conservative numerical flux for the Eqn. (1.1) are given by,

$$\hat{\mathbf{F}}^x_{i+1/2,j} = \begin{Bmatrix} \hat{\mathbf{F}}^x_{i,i+1/2,j} \\ \hat{\mathbf{F}}^x_{e,i+1/2,j} \\ \hat{\mathbf{F}}^x_{m,i+1/2,j} \end{Bmatrix}, \qquad \hat{\mathbf{F}}^y_{i,j+1/2} = \begin{Bmatrix} \hat{\mathbf{F}}^y_{i,j+1/2} \\ \hat{\mathbf{F}}^y_{e,i,j+1/2} \\ \hat{\mathbf{F}}^y_{m,i,j+1/2} \end{Bmatrix}. \tag{3.9}$$

3.2. **Numerical diffusion operator.** As entropy is dissipated at shocks, we need to add *entropy stable* numerical diffusion operators to avoid spurious oscillations at shocks. Following [18],the resulting numerical fluxes are of the form,

$$\mathbf{F}^x_{i+1/2,j} = \hat{\mathbf{F}}^x_{i+1/2} - \frac{1}{2}\mathbf{D}^x_{i+1/2}[\mathbf{V}]_{i+1/2,j}, \qquad \mathbf{F}^y_{i,j+1/2} = \hat{\mathbf{F}}^x_{i+1/2} - \frac{1}{2}\mathbf{D}^y_{i,j+1/2}[\mathbf{V}]_{i,j+1/2}. \tag{3.10}$$

with diffusion matrices are given by,

$$\mathbf{D}^x_{i+1/2} = R^x_{i+1/2,j}\Lambda^x_{i+1/2,j}R^{x\top}_{i+1/2,j}, \qquad \mathbf{D}^y_{i,j+1/2} = R^y_{i,j+1/2}\Lambda^y_{i,j+1/2}R^{y\top}_{i,j+1/2}. \tag{3.11}$$

Here $R^{\{x,y\}}$ are the matrices of right eigenvectors of jacobians $\partial_{\mathbf{u}}\mathbf{f}^{\{x,y\}}$ and $\Lambda^{\{x,y\}}$ are diagonal matrices of eigenvalues in the x- and y-directions, respectively. We will use a Rusanov type type diffusion operator given by a 18×18 matrix,

$$\Lambda^{\{x,y\}} = \Lambda = \text{diag}\{(\max_{1\le i\le 5}|\lambda^x_i|)I_{5\times 5}, (\max_{6\le i\le 10}|\lambda^x_i|)I_{5\times 5}, (\max_{1\le i\le 18}|\lambda^x_i|)I_{8\times 8}\}.$$

We use the eigenvector scaling due to Barth [4] for defining the eigenvector matrices.

3.3. **Second Order Dissipation Operator.** The diffusion operators described above are of first order, as the jump term $[\mathbf{V}]$ is of order Δx. To obtain the second order accurate scheme, we can perform piecewise linear reconstructions of the entropy variable $\mathbf{V}$. However, a straightforward reconstruction of the entropy variables may not be entropy stable. In [6], the authors have constructed entropy stable second order (and even higher-order) diffusion operators. For simplicity, we will consider the diffusion operator, $\mathbf{D}^x_{i+1/2,j}[\mathbf{V}]_{i+1/2,j}$ in x-direction only. The diffusion operator in y-direction, $\mathbf{D}^y_{i,j+1/2}[\mathbf{V}]_{i,j+1/2}$ can be constructed analogously. We need to introduce *scaled* entropy variables,

$$\mathbf{W}^{x,\pm}_{i,j} = R^{x\top}_{i\pm 1/2,j}\mathbf{V}_{i,j}.$$

If $\tilde{\mathbf{W}}^{x,\pm}_{i,j}$ are the reconstructed values of $\mathbf{W}^{x\pm}$ in the x-direction, then the corresponding reconstructed values $\mathbf{P}^{x\pm}_i$ for $\mathbf{V}_{ij}$ are given by,

$$\mathbf{P}^{x\pm}_{ij} = \{R^{xT}_{i\pm i+1/2,j}\}^{(-1)}\tilde{\mathbf{W}}^{x,\pm}_{i,j}.$$

The resulting second order entropy stable flux is then given by,

$$\mathbf{F}^x_{i+1/2,j} = \hat{\mathbf{F}}^x_{i+1/2} - \frac{1}{2}\mathbf{D}^x_{i+1/2}[\mathbf{P}^x]_{i+1/2,j}, \tag{3.12}$$

where the jump term $[\mathbf{P}^x]_{i+1/2,j}$ is given by,

$$[\mathbf{P}^x]_{i+1/2,j} = \mathbf{P}^{x-}_{i+1,j} - \mathbf{P}^{x+}_{i,j}.$$

A sufficient condition for the scheme to be entropy stable (see [6]) is the existence of a diagonal matrix $B^x \ge 0$, such that,

$$[\tilde{\mathbf{W}}^x]_{i+1/2,j} = B^x_{i+1/2,j}[\mathbf{W}^x]_{i+1/2,j},$$

i.e. the reconstruction of $\mathbf{W}^x$ has to satisfy a *sign preserving property* along the interfaces of each cell. Component-wise this can be written as,

$$\text{sign}([\tilde{w}^l]) = \text{sign}([w^l]), \tag{3.13}$$

for each component w^l and $\tilde{w}^l$ of $\mathbf{W}^x$ and $\tilde{\mathbf{W}}^x$, respectively.

3.4. **Reconstruction Procedure.** We suppress the j-dependence below for notational convenience. The reconstruction for $\mathbf{W}^x$ is performed component-wise, so that (3.13) is satisfied. Let us define jump of component w of the variable $\mathbf{W}^x$,

$$\delta_{i+1/2} = [w]_{i+1/2}. \tag{3.14}$$

Consider ϕ, a slope limiter satisfying $\phi(\theta^{-1}) = \phi(\theta)\theta^{-1}$ and define divided differences,

$$\theta_i^- = \frac{\delta_{i+1/2}}{\delta_{i-1/2}} \quad \text{and} \quad \theta_i^+ = \frac{\delta_{i-1/2}}{\delta_{i+1/2}}.$$

Then the reconstructed values of w in the cell I_i are

$$\tilde{w}_i^- = w_i^- - \frac{1}{2}\phi(\theta_i^-)\delta_{i-1/2}, \qquad \tilde{w}_i^+ = w_i^+ + \frac{1}{2}\phi(\theta_{i+1}^+)\delta_{i+1/2}.$$

Using these values we obtain

$$[\tilde{w}]_{i+1/2} = \left(1 - \frac{1}{2}(\phi(\theta_i^+) + \phi(\theta_{i+1}^-))\right)\delta_{i+1/2}.$$

This shows that the sign property is satisfied iff

$$\phi(\theta) \leq 1, \quad \forall\ \theta \in \mathbb{R}.$$

In this article, we will use the minmod limiter based reconstruction which satisfies the sign preserving property (see [6]). The minmod limiter is given by,

$$\phi(\theta) = \begin{cases} 0, & \text{if } \theta < 0, \\ \theta, & \text{if } 0 \leq \theta \leq 1, \\ 1, & \text{else.} \end{cases} \tag{3.15}$$

3.5. **Discrete entropy stability.** In this section, we prove that scheme given by the flux (3.12) is entropy stable i.e. it satisfies a discrete version of the entropy estimate (2.3). We have the following result,

Theorem 3.1. *The semi-discrete finite difference scheme* (3.2)*, with entropy stable numerical flux* (3.12)*, is second order accurate for smooth solutions. Furthermore, it satisfy,*

$$\frac{d}{dt}\sum_{i,j}(e_{i,i,j} + e_{e,i,j} + e_{m,i,j})\Delta x\Delta y \leq C_5 \sum_{i,j}(e_{i,i,j} + e_{e,i,j} + e_{m,i,j})\Delta x\Delta y + C_6 \tag{3.16}$$

if conditions for Theorem 2.1 are satisfied.

Proof. It is easy to see that the scheme is of second order accuracy, as both the entropy conservative flux $\hat{\mathbf{F}}$ and the numerical diffusion operator, are second order accurate for smooth solutions. Now, consider the fluid part of (3.2), i.e.

$$\frac{d\mathbf{U}_{\alpha,i,j}}{dt} + \frac{1}{\Delta x}\left(\mathbf{F}^x_{\alpha,i+1/2,j} - \mathbf{F}^x_{\alpha,i-1/2,j}\right) + \frac{1}{\Delta y}\left(\mathbf{F}^y_{\alpha,i,j+1/2} - \mathbf{F}^y_{\alpha,i,j-1/2}\right) = \mathbf{S}_{\alpha,i,j}(\mathbf{U}), \tag{3.17}$$

for $\alpha \in \{i, e\}$ with *entropy numerical fluxes*,

$$\mathbf{Q}^x_{i+1/2,j} = \overline{\mathbf{V}}^\top_{i+1/2,j}\mathbf{F}^x_{i+1/2,j} - \bar{\chi}_{i+1/2,j}, \qquad \mathbf{Q}^y_{i,j+1/2} = \overline{\mathbf{V}}^\top_{i,j+1/2}\mathbf{F}^y_{i,j+1/2} - \bar{\chi}_{i,j+1/2}. \tag{3.18}$$

Multiplying (3.17) with $\mathbf{V}^\top_{\alpha,i,j}$ and imitating the proof of Theorem 2.2 form [17], we get

$$\begin{aligned} \frac{de_\alpha(\mathbf{U}_{i,j})}{dt} &= \frac{1}{\Delta x}\left(\hat{\mathbf{Q}}^x_{i+1/2,j} - \hat{\mathbf{Q}}^x_{i-1/2,j}\right) - \frac{1}{\Delta x}\left(\hat{\mathbf{Q}}^y_{i,j+1/2} - \hat{\mathbf{Q}}^y_{i,j-1/2}\right) + \mathbf{V}^\top_{\alpha,i,j}\mathbf{S}_{\alpha,i,j}(\mathbf{U}) \\ &- \frac{1}{2\Delta x}\left([\mathbf{V}]^\top_{i+1/2,j}\mathbf{D}^x_{i+1/2,j}[\mathbf{P}^x]_{i+1/2,j} + [\mathbf{V}]^\top_{i-1/2,j}\mathbf{D}^x_{i-1/2,j}[\mathbf{P}^x]_{i-1/2,j}\right) \end{aligned}$$

$$
\begin{aligned}
- & \frac{1}{2\Delta y}\left([\mathbf{V}]^\top_{i,j+1/2}\mathbf{D}^y_{i,j+1/2}[\mathbf{P}^y]_{i,j+1/2} + [\mathbf{V}]^\top_{i,j-1/2}\mathbf{D}^y_{i,j-1/2}[\mathbf{P}^y]_{i,j-1/2}\right)\\
= & -\frac{1}{\Delta x}\left(\mathbf{Q}^x_{i+1/2,j} - \mathbf{Q}^x_{i-1/2,j}\right) - \frac{1}{\Delta x}\left(\mathbf{Q}^y_{i,j+1/2} - \mathbf{Q}^y_{i,j-1/2}\right) + \mathbf{V}^\top_{\alpha,i,j}\mathbf{S}_{\alpha,i,j}(\mathbf{U})\\
- & \frac{1}{4\Delta x}\left([\mathbf{V}]^\top_{i+1/2,j}\mathbf{D}^x_{i+1/2,j}[\mathbf{P}^x]_{i+1/2,j} + [\mathbf{V}]^\top_{i-1/2,j}\mathbf{D}^x_{i-1/2,j}[\mathbf{P}^x]_{i-1/2,j}\right)\\
- & \frac{1}{4\Delta y}\left([\mathbf{V}]^\top_{i,j+1/2}\mathbf{D}^y_{i,j+1/2}[\mathbf{P}^y]_{i,j+1/2} + [\mathbf{V}]^\top_{i,j-1/2}\mathbf{D}^y_{i,j-1/2}[\mathbf{P}^y]_{i,j-1/2}\right)
\end{aligned}
$$

Here

$$\hat{\mathbf{Q}}^x_{i+1/2,j} = \overline{\mathbf{V}}^\top_{i+1/2,j}\hat{\mathbf{F}}^x_{i+1/2,j} - \bar{\chi}_{i+1/2,j}, \text{ and } \hat{\mathbf{Q}}^y_{i,j+1/2} = \overline{\mathbf{V}}^\top_{i,j+1/2}\hat{\mathbf{F}}^y_{i,j+1/2} - \bar{\chi}_{i,j+1/2}.$$

are entropy fluxes corresponding to the entropy conservative fluxes $\hat{\mathbf{F}}^x$ and $\hat{\mathbf{F}}^y$ respectively. Let us consider the diffusion terms. Ignoring all the indices, each diffusion term satisfy,

$$
\begin{aligned}
[\mathbf{V}]^\top\mathbf{D}[\mathbf{P}] &= [\mathbf{V}]^\top R\Lambda R^\top[\mathbf{P}]\\
&= [\mathbf{V}]^\top R\Lambda R^\top(R^\top)^{(-1)}[\tilde{\mathbf{W}}]\\
&= (R^\top[\mathbf{V}])^\top\Lambda B([\mathbf{W}])\\
&= (R^\top[\mathbf{V}])^\top\Lambda B(R^\top\mathbf{V})\\
&\geq 0,
\end{aligned}
$$

as both B and Λ are non-negative diagonal matrices. So, we get

$$\frac{de_{\alpha,i,j}}{dt} + \frac{1}{\Delta x}\left(\mathbf{Q}^x_{\alpha,i+1/2,j} - \mathbf{Q}^x_{\alpha,i-1/2,j}\right) + \frac{1}{\Delta y}\left(\mathbf{Q}^y_{\alpha,i,j+1/2} - \mathbf{Q}^y_{\alpha,i,j-1/2}\right) \leq \mathbf{V}^\top_{\alpha,i,j}\mathbf{S}_{\alpha,i,j}.$$

A simple calculation shows that,

$$\mathbf{V}^\top_{\alpha,i,j}\mathbf{S}_{\alpha,i,j} = 0.$$

This results in the fluid entropy inequality,

$$\frac{de_{\alpha,i,j}}{dt} + \frac{1}{\Delta x}\left(\mathbf{Q}^x_{\alpha,i+1/2,j} - \mathbf{Q}^x_{\alpha,i-1/2,j}\right) + \frac{1}{\Delta y}\left(\mathbf{Q}^y_{\alpha,i,j+1/2} - \mathbf{Q}^y_{\alpha,i,j-1/2}\right) \leq 0, \quad \alpha \in \{i,e\}, \tag{3.19}$$

summing over all the cells we get,

$$\frac{d}{dt}\sum_{i,j} e_{\alpha,i,j}\Delta x\Delta y \leq 0, \quad \alpha \in \{i,e\}, \tag{3.20}$$

Repeating the entropy argument of Dafermos [5] used in Theorem 2.1 we get an discrete energy estimate for fluid part,

$$\sum_{i,j}\left(\rho^2_{\alpha,i,j} + |\rho_{\alpha,i,j}\mathbf{v}_{\alpha,i,j}|^2 + E^2_{\alpha,i,j}\right)\ \Delta x\Delta y \leq C_7\sum_{i,j} e_{\alpha,i,j}\Delta x\Delta y + C_8, \tag{3.21}$$

Imitating the proof of Theorem 2.1 where integration is replaced by summation, we get,

$$\frac{d}{dt}\sum_{i,j} e_{m,i,j}\Delta x\Delta y \leq C_9\sum_{i,j}(e_{m,i,j} + e_{i,i,j} + e_{e,i,j})\Delta x\Delta y + C_{10}. \tag{3.22}$$

Combining with (3.20), we get (3.16). □

order	α_{il}			β_{il}		
2	1			1		
	1/2	1/2		0	1/2	
3	1			1		
	3/4	1/4		0	1/4	
	1/3	0	2/3	0	0	2/3

TABLE 1. Parameters for Runge-Kutta time marching schemes.

4. Fully Discrete Schemes

Let $\mathbf{U}^n$ is the discrete solution at t^n, and $\Delta t = t^{n+1} - t^n$. Then a semi-discrete scheme (3.2) can be written as,

$$\frac{d\mathbf{U}^n_{i,j}}{dt} = \mathcal{L}_{i,j}(\mathbf{U}^n) + \mathbf{S}_{i,j}(\mathbf{U}^n), \tag{4.1}$$

where,

$$\mathcal{L}_{i,j}(\mathbf{U}^n) = -\frac{1}{\Delta x}\left(\mathbf{F}^x_{i+1/2,j} - \mathbf{F}^x_{i-1/2,j}\right) - \frac{1}{\Delta y}\left(\mathbf{F}^y_{i,j+1/2} - \mathbf{F}^y_{i,j-1/2}\right), \text{ and } \mathbf{S}_{i,j}(\mathbf{U}^n) = \mathbf{s}(\mathbf{U}^n_{i,j}).$$

We describe two different time discretization schemes below.

4.1. Explicit Schemes.

We use explicit Runge-Kutta (RK) time marching schemes for the time-discretizing of the two-fluid equations. For simplicity, we restrict ourselves to the second- and third-order accurate RK schemes (see [16]). These methods are strong stability preserving (SSP). In order to advance a numerical solution from time t^n to t^{n+1}, the SSP-RK algorithm is as follows:

1. Set $\mathbf{U}^{(0)} = \mathbf{U}^n$.
2. For $m = 1, ..., k+1$, compute,
$$\mathbf{U}^{(m)}_{i,j} = \sum_{l=0}^{m-1} \alpha_{ml}\mathbf{U}^{(l)}_{i,j} + \beta_{ml}\Delta t^n(\mathcal{L}_{i,j}(\mathbf{U}^{(l)}) + \mathbf{S}_{i,j}(\mathbf{U}^{(l)})).$$
3. Set $\mathbf{U}^{n+1}_{i,j} = \mathbf{U}^{(k+1)}_{i,j}$.

The coefficients α_{ml} and β_{ml} are given in Table 1.

4.2. IMEX-RK Schemes.

As the source term in two-fluid equations is stiff, the explicit time stepping scheme works only for a very restricted time step. Hence, we consider IMEX methods. An Implicit-Explicit Runge-Kutta (IMEX-RK) scheme for (1.1), is based on the implicit treatment of the stiff source term and and an explicit treatment of the convective flux terms. We will use SSP-RK schemes described above for the explicit time-stepping, with each intermediate Euler update is carried out by solving,

$$\mathbf{U}^{m+1}_{i,j} = \mathbf{U}^m_{i,j} + \Delta t\mathcal{L}_{i,j}(\mathbf{U}^m) + \Delta t\mathbf{S}_{i,j}(\mathbf{U}^{m+1}), \tag{4.2}$$

for $\mathbf{U}^{m+1}$. Usually (4.2) is solved using some iterative methods. However, we can exploit the special structure of the source term for the two-fluid equations to solve (4.2) exaclty. We proceed as follows:

Denote $\mathbf{U} = \{\mathbf{W}_1, \mathbf{W}_2, \mathbf{W}_3\}$ with,

$$\mathbf{W}_1 = \{\rho_i, \rho_e, B^x, B^y, B^z, \psi\}^\top$$

$$\begin{aligned}\mathbf{W}_2 &= \{\rho_i v_i^x, \rho_i v_i^y, \rho_i v_i^z, \rho_e v_e^x, \rho_e v_e^y, \rho_e v_e^z, E^x, E^y, E^z\}^\top \\ \mathbf{W}_3 &= \{E_i, E_e, \phi\}^\top\end{aligned}$$

We observe that (4.2) can be rewritten in the following three blocks,

$$\mathbf{W}_1^{(m+1)} = \mathbf{G}_1(\mathbf{U}^{(m)}), \tag{4.3a}$$

$$\mathbf{W}_2^{(m+1)} = \mathbf{G}_2(\mathbf{U}^{(m)}) + \mathcal{A}(\mathbf{W}_1^{(m+1)})\mathbf{W}_2^{(m)}, \tag{4.3b}$$

$$\mathbf{W}_3^{(m+1)} = \mathbf{G}_3(\mathbf{U}^{(m)}) + \mathbf{H}(\mathbf{W}_1^{(m+1)}, \mathbf{W}_2^{(m+1)}). \tag{4.3c}$$

Here $\mathbf{G}_1, \mathbf{G}_2$ and $\mathbf{G}_3$ are the explicit parts of (4.2) for the variables $\mathbf{W}_1, \mathbf{W}_2$ and $\mathbf{W}_3$ respectively. The Eqns. (4.3) are then solved in sequential manner:

I) Equation (4.3a) is updated explicitly, as it involves the evaluation of the known terms from the previous time step.

II) Note that the matrix $\mathcal{A}(\mathbf{W}_1^{(m+1)})$ in Eqn. (4.3b) is,

(4.4)
$$\begin{bmatrix}
0 & \frac{B^{z,(m+1)}}{\hat{r}_g} & -\frac{B^{y,(m+1)}}{\hat{r}_g} & 0 & 0 & 0 & \frac{\rho_i^{(m+1)}}{\hat{r}_g} & 0 & 0 \\
-\frac{B^{z,(m+1)}}{\hat{r}_g} & 0 & \frac{B^{x,(m+1)}}{\hat{r}_g} & 0 & 0 & 0 & 0 & \frac{\rho_i^{(m+1)}}{\hat{r}_g} & 0 \\
\frac{B^{y,(m+1)}}{\hat{r}_g} & -\frac{B^{x,(m+1)}}{\hat{r}_g} & 0 & 0 & 0 & 0 & 0 & 0 & \frac{\rho_i^{(m+1)}}{\hat{r}_g} \\
0 & 0 & 0 & 0 & \frac{B^{z,(m+1)}}{\hat{r}_{e,g}} & -\frac{B^{y,(m+1)}}{\hat{r}_{e,g}} & \frac{\rho_e^{(m+1)}}{\hat{r}_{e,g}} & 0 & 0 \\
0 & 0 & 0 & -\frac{B^{z,(m+1)}}{\hat{r}_{e,g}} & 0 & \frac{B^{x,(m+1)}}{\hat{r}_{e,g}} & 0 & \frac{\rho_e^{(m+1)}}{\hat{r}_{e,g}} & 0 \\
0 & 0 & 0 & \frac{B^{y,(m+1)}}{\hat{r}_{e,g}} & -\frac{B^{x,(m+1)}}{\hat{r}_{e,g}} & 0 & 0 & 0 & \frac{\rho_e^{(m+1)}}{\hat{r}_{e,g}} \\
\frac{-r_i}{K} & 0 & 0 & \frac{-r_e}{K} & 0 & 0 & 0 & 0 & 0 \\
0 & \frac{-r_i}{K} & 0 & 0 & \frac{-r_e}{K} & 0 & 0 & 0 & 0 \\
0 & 0 & \frac{-r_i}{K} & 0 & 0 & \frac{-r_e}{K} & 0 & 0 & 0
\end{bmatrix}$$

with $\hat{r}_{e,g} = -\hat{r}_g/\lambda_m$ and $K = \hat{\lambda}^2 \hat{r}_g$. All the quantities in the matrix are already computed in step I. So, we can rewrite Eqn. (4.3b) as,

$$\mathbf{W}_2^{(m+1)} = \left(\mathbf{I} - (\Delta t)\mathcal{A}(\mathbf{W}_1^{(m+1)})\right)^{(-1)} \mathbf{G}_2(\mathbf{U}^{(m)}). \tag{4.5}$$

which can evaluated exactly.

III) The Eqn. (4.3c) is now updated for $\mathbf{W}_3^{m+1}$ by evaluating $\mathbf{H}(\mathbf{W}_1^{m+1}, \mathbf{W}_2^{m+1})$.

Thus, our IMEX scheme does not require any non-linear Newton solves or any global matrix inversions. It only needs explicit evaluations of the inverse of a local 9×9 matrix in each cell making this scheme computationally inexpensive.

5. Numerical Results

We present a set of numerical experiments to demonstrate the robustness of the proposed schemes.

5.1. Convergence Rates.

As it is not possible to obtain explicit solution formulas for the two-fluid equations, we employ a forced solution approach to manufacture explicit solutions.

In one space dimension, we consider the *modified* equation:

$$\partial_t \mathbf{u} + \partial_x \mathbf{f}(\mathbf{u}) = \mathbf{s}(\mathbf{u}) + K(x,t).$$

with forcing term:

$$K(x,t) = \{\mathbf{0}_{13}, -(2 + \sin(2\pi(x-t))), 0, 0, 2 + \sin(2\pi(x-t)), 0\}^\top$$

The initial densities are $\rho_i = \rho_e = 2.0 + \sin(2\pi x)$, with the velocities $v_i^x = v_e^x = 1.0$ and the pressures $p_i = p_e = 1.0$. The initial magnetic field is $B^y = \sin(2\pi x)$ and the electric field is

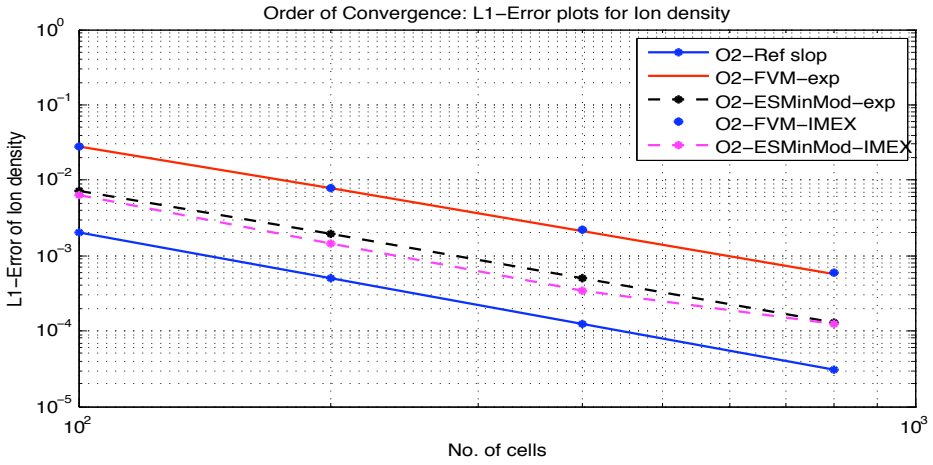

FIGURE 1. L^1 order of convergence: L^1-errors of the ion-density at time $t = 2.0$ are plotted for 100, 200, 400, and 800 cells.

$E^z = -\sin(2\pi x)$. The computational domain is $(0, 1)$ with periodic boundary conditions. To ensure non-vanishing source term we take ion-electron mass ratio to be $m_i/m_e = 2.0$.

It is straightforward to check that the exact solution is

$$\rho_i = \rho_e = 2.0 + \sin(2\pi(x - t)).$$

In Figure 1, we have plotted the convergence rates for the second-order schemes based on entropy stable fluxes with minmod (ES-MinMod) reconstruction for the spatial discretization and the second order SSP-RK scheme for time update. For comparison, we have also plotted the results for the second-order FVM scheme based on a four wave HLL type solver with minmod limiter (O2-FVM). We observe that entropy stable scheme are less diffusive than the standard FVM schemes. The IMEX schemes also perform equally well. However, we observe that rate of convergence for IMEX scheme falls when we refine the mesh. This is due to splitting errors for the IMEX schemes.

5.2. **Soliton Propagation in One Dimension.** Soliton propagation in two-fluid plasmas are simulated in [9, 1, 3, 2]. It is shown that ion-acoustic solitons can form from an initial density hump. In this section, we follow [9, 3], to simulate this soliton in one dimension with ion-electron mass ratio of 25. Then, we simulate soliton with realistic ion-electron mass-ratio of 1836.

5.2.1. *Soliton Propagation in One Dimension: Low mass ratio.*

No. of Cells	O2-ESMN-exp	O2-ESMN-IMEX
100	18.58	5.97
200	37.12	24.02
400	93.86	96.37
800	378.54	386.9

TABLE 2. Comparison of simulation times of numerical scheme at various resolution.

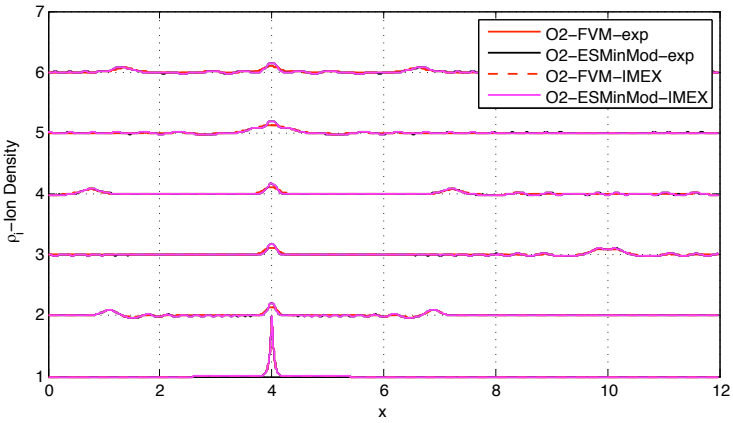

(a) Ion-dnesity evolution: Ion-density at non-dimensional $t = 0, 1, 2, 3, 4$, and 5

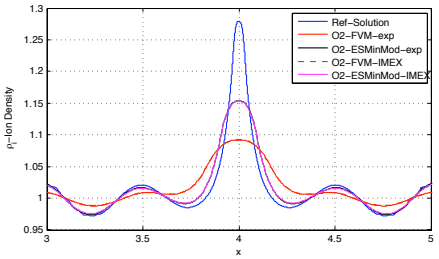

(b) Ion-density plot for various schemes: Zoomed at $x = 4.0$ wave at non-dimensional time $t = 5.0$

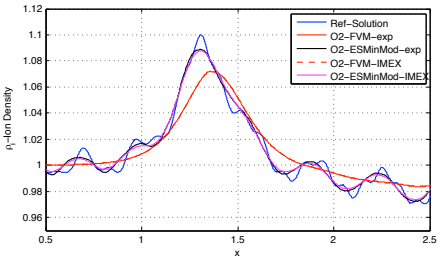

(c) Ion-density plot for various schemes: Zoomed at $x = 1.5$ at non-dimensional time $t = 5.0$

FIGURE 2. Soliton propagation in one dimensions

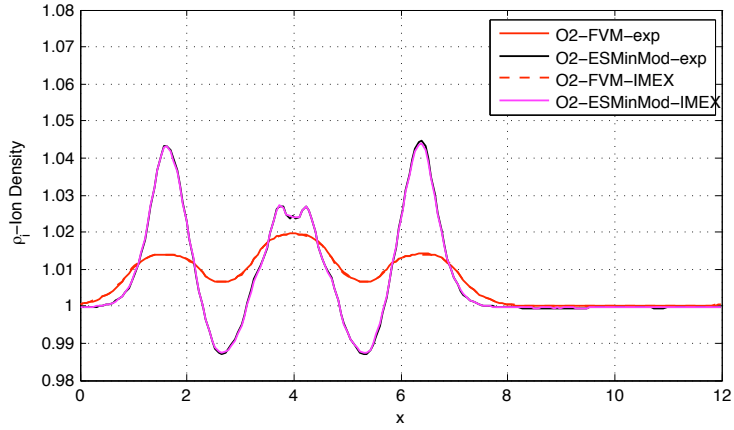

FIGURE 3. Soliton propagation: Numerical solutions at under-resolved meshes of 200 cells.

Initially, the plasma is assumed to be stationary with ion density,

$$\rho_i = 1.0 + \exp(-25.0|x - L/3.0|) \tag{5.1}$$

and mass ratio $m_i/m_e = 25$ on the computational domain $D = (0, L)$ with $L = 12.0$. Electron pressure is $p_e = 5.0\rho_i$ with ion-electron pressure ratio of 1/100. Normalized Debye length is taken to be 1.0 and normalized Larmor radius is 0.01. Periodic boundary conditions are used.

Numerical results are presented in fig. 2 for the second order schemes with explicit and IMEX time-stepping, using 2000 cells. The solutions are plotted for second order entropy stable schemes O2-ESMN. For comparison, we have also computed the solution with standard FVM scheme O2-FVM. In Figure 2(a), we have plotted the ion-density profile at non-dimensional times $t = 0, 1, 2, 3, 4$ and 5. Observe that all the schemes are able to capture soliton waves. In particular, the speed of soliton propagation is the same for all the schemes. In Figure 2(b), we have zoomed at the the stationary central wave ($atx = 4.0$) of the solution after time $t = 5.0$ and compared the schemes. We have also plotted a reference solution computed using O2-FVM-exp scheme on 40000 cells. We observe that the entropy stable schemes are more accurate than the standard FVM scheme. Furthermore, both explicit and IMEX time-stepping gives similar results. Similar features can be observed from Figure 2(c) where we have plotted the left wave (at $x = 1.0$) at time $t = 5$. In Figure 3, we have plotted the solution at the under-resolved mesh of 200 cells. At this low resolution, the time step is constrained due to the source term. We again observe that the entropy stable schemes are less diffusive than the FVM scheme. However observe that the middle stationary wave is not fully resolved by both the explicit and IMEX schemes.

In Table 2, we have presented the simulation time in seconds for the second order entropy stable schemes at various resolutions. At lower resolutions (No of cells less than 200), the time step is dictated by the source terms, so the IMEX schemes are faster. In fact, we observe that at the resolution of 100 cells, IMEX schemes are almost three times faster than the corresponding explicit scheme. However, as we compute for finer resolutions, the CFL condition (in terms of the wave speeds) dictates the time step. So, the simulation times of both types of schemes becomes comparable.

5.2.2. *Soliton Propagation in One Dimension: Realistic Mass Ratio.* In this section, we simulate the soliton propagation with realistic ion-electron mass ratio i.e. with $m_i/m_e = 1836$. The initial ion-density is

$$\rho_i = (1.0 + M \exp(-25.0|x - L/3.0|)) \tag{5.2}$$

with $M = 2.0$ on the computational domain $(0, L_x)$ with $L_x = 12.0$. All other initial and boundary conditions are the same as in the case of one-dimensional soliton propagation in section 5.2.1. We need about 10000 cells to resolve all the small scale oscillations.

Numerical results are plotted in Figure 4 for the second order ES-MinMod scheme, using both explicit and IMEX time-stepping procedures. In Figure 4(a), we have plotted the ion density at non-dimensional times $t = 0, 1, 2, 3, 4$ and 5. We observe that both IMEX and explicit schemes captures the soliton waves equally well. Also, note that the soliton waves have accelerated after passing through the stationary wave. The acceleration is directly proportional to the magnitude M of the perturbation to the density. In Figure, 4(b) we have zoomed at central stationary wave. Note that both schemes have resolved small scale oscillations. We would also like to point out that it is possible to run simulations at lower resolutions. However, this leads to unresolved oscillations similar to the case of the under-resolved simulation in section 5.2.1 (see Figure 3).

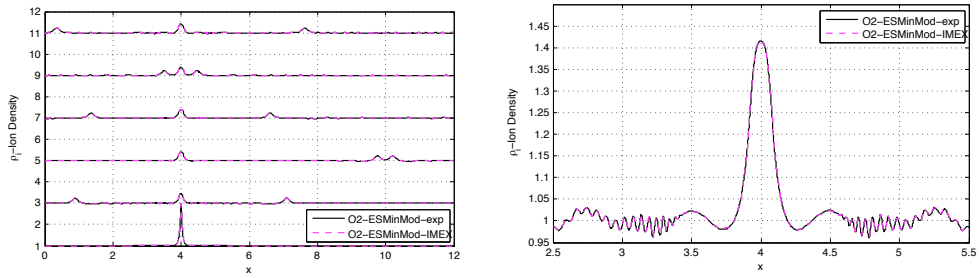

(a) Ion-density evolution: Ion-density at non-dimensional $t = 0, 1, 2, 3, 4$, and 5

(b) Ion-density plot for various schemes: Zoomed at the central stationary wave at non-dimensional time $t = 5.0$

FIGURE 4. Soliton propagation with ion-electron mass ratio $m_i/m_e = 1836$ in one dimension

5.3. **Generalized Brio-Wu Shock tube Problem.** The initial conditions for this Riemann problem are

$$\mathbf{U}_{\text{left}} = \begin{cases} \rho_i = 1.0 \\ p_i = 5 \times 10^{-5} \\ \rho_e = 1.0 \ m_e/m_i \\ p_e = 5 \times 10^{-5} \\ B^x = 0.75 \\ B^y = 1.0 \\ \mathbf{v}_i = \mathbf{v}_e = \mathbf{E} = 0 \\ \phi = \psi = B^z = 0 \end{cases} \qquad \mathbf{U}_{\text{right}} = \begin{cases} \rho_i = 0.125 \\ p_i = 5 \times 10^{-6} \\ \rho_e = 0.125 \ m_e/m_i \\ p_e = 5 \times 10^{-6} \\ B^x = 0.75 \\ B^y = -1.0 \\ \mathbf{v}_i = \mathbf{v}_e = \mathbf{E} = 0 \\ \phi = \psi = B^z = 0 \end{cases} \tag{5.3}$$

on the computational domain $(0, 1)$ with, $\mathbf{U} = \mathbf{U}_{\text{left}}$ for $x < 0.5$ and $\mathbf{U} = \mathbf{U}_{\text{right}}$ for $x > 0.5$. The ion-electron mass ratio is taken to be $m_i/m_e = 1836$. The initial condition are non-dimensionzed using $p_0 = 10^{-4}$. Non-dimensional Debye length is taken to be 0.01. Simulations are carried out using Larmor radii of 10 and 0.001. Neumann boundary conditions are used.

Numerical solutions are presented in Figure 5. In Figure 5(a) we have plotted the numerical solutions based on O2-ESMinMod scheme using second order explicit and IMEX time updates. Solutions are computed with non-dimensional Larmor radius of 10.0 using 1000 cells. We observe that solution is close to the Euler solution. Furthermore, both IMEX and explicit schemes produce similar results.

In Figure 5(b) we have plotted the solutions with non-dimensional Larmor radius of 0.001. Numerical solutions are computed using 50000 cells. The number of cells may seems too excessive but they are needed in order to resolve the small scale oscillations, present in the solution due to the physics of the problem. We observe that the both explicit and IMEX solutions are converging to the MHD limit. In fact, explicit schemes have resolved all the waves. However it produces some small scale oscillations. On the other hand, the IMEX scheme do not resolve the middle contact discontinuity correctly. For explicit scheme, the small scale oscillation disappear when SSP-RK3 time update is used(see Figure 5(c)). However, similar to the case of SSP-RK2, the third order SSP-RK3 IMEX scheme does not resolve the contact discontinuity. This points to the need of developing more suitable IMEX-RK schemes for two-fluid equations.

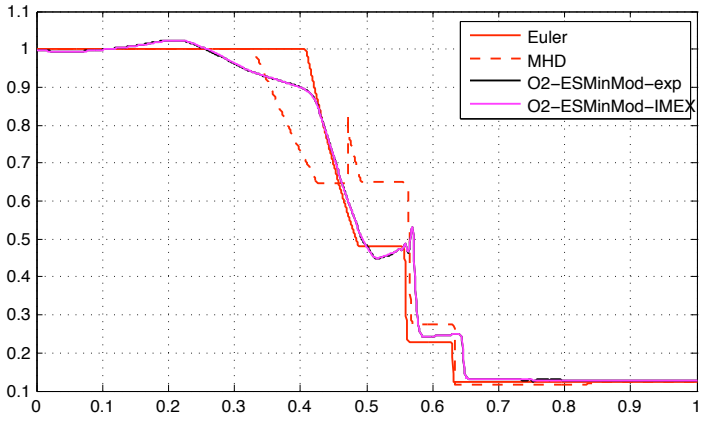

(a) Generalized Brio-Wu shock tube problem: 1000 cells were used. Numerical solutions are plotted for $\hat{r}_g = 10.0$

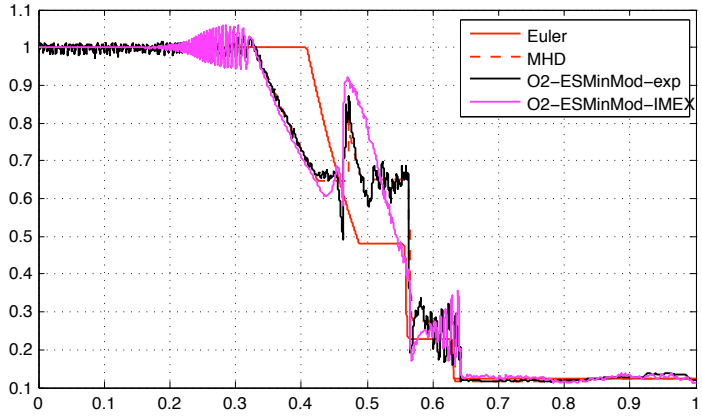

(b) Generalized Brio-Wu shock tube problem: 50000 cells were used. Numerical solutions are plotted for second order schemes with $\hat{r}_g = 0.001$

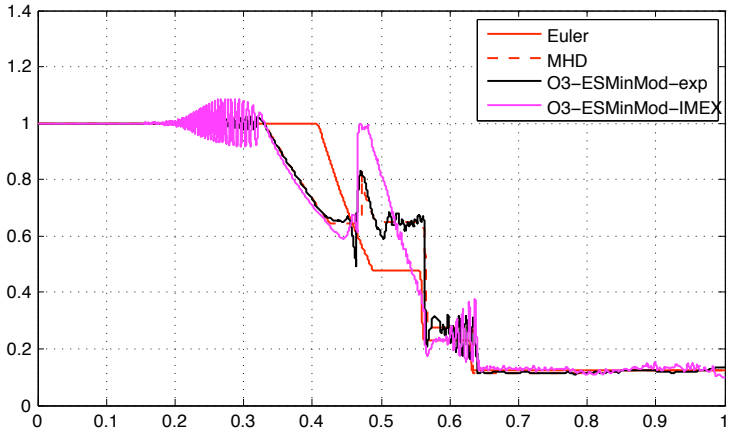

(c) Generalized Brio-Wu shock tube problem: 50000 cells were used. Numerical solutions are plotted for second order schemes with $\hat{r}_g = 0.001$

FIGURE 5. Generalized Brio-Wu shock tube Riemann problem

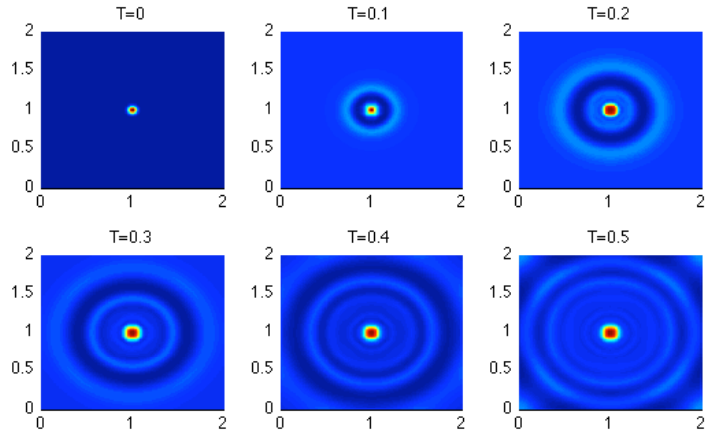

(a) Ion-denisty evolution:Ion density ρ_i at time $t = 0.0, 0.1, 0.2, 0.3, 0.4$, and 0.5

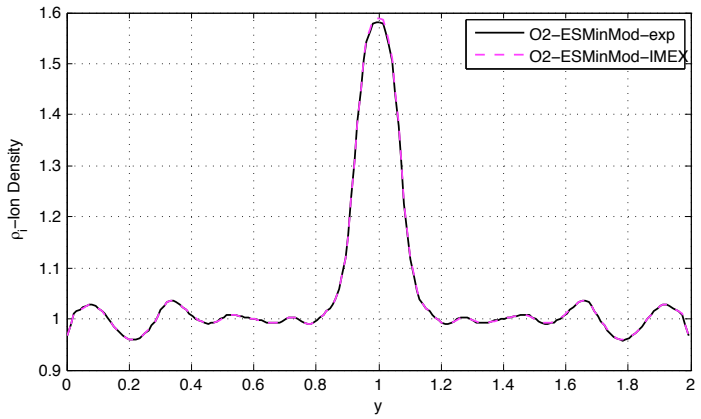

(b) Comparison of the schemes: Ion-density cut at $x = 1$ for time $t = 0.5$ of various schemes

FIGURE 6. Soliton propagation in two dimensions

5.4. **Soliton Propagation in Two space dimensions.** Initial ion-density of the plasma is considered to be,

$$\rho_i = 1.0 + 5.0 \exp(-500.0((x - L_x/2.0)^2 + (y - L_y/2.0)^2) \tag{5.4}$$

on the computational domain $(0, L_x)\times(0, L_y)$ with $L_x = L_y = 2.0$. All other initial conditions are same as in the case of one dimensional soliton propagation in section 5.2.1. Neumann boundary conditions are used to allow the waves to exit the domain without noticeable reflections. Note that this simulation is more stiff than those carried out in [2].

Numerical results are presented Figure 6. In Figure 6(a) we have plotted the solution at non-dimensional time of $t = 0, 0.1, 0.2, 0.3, 0.4$ and 0.5 using second order entropy stable scheme with IMEX time stepping (O2-ESMN-IMEX). We observe that soliton structures similar to the one dimensional forming and moving away from the central density hump. In Figure 6(b) we have

one dimensional plots of the solutions at $x = 1$ at time $t = 0.5$ for explicit and IMEX schemes. The performance of both explicit and IMEX schemes is comparable.

6. Conclusion

We have presented second-order, entropy stable finite difference schemes for the ideal two-fluid MHD equations. The semi-discrete version of the schemes is shown to be entropy stable. Furthermore, entropy stable schemes are shown to be more accurate (less diffusive) than the FVM schemes using several benchmark examples. To overcome the time-step restriction imposed by stiff source term, we have designed computationally efficient IMEX schemes. The proposed schemes are shown to be robust in a series of numerical experiments.

References

[1] Baboolal, S., Finite-difference modeling of solitons induced by a density hump in a plasma multi-fluid. Math. and Comp. in Simulation, Vol. 55, 309-316 (2001)
[2] Baboolal, S., High-resolution numerical simulation of 2D nonlinear wave structures in electromagnetic fluids with absorbing boundary conditions. J. Comp. Appl. Math., Vol. 234, 1710-1716 (2010)
[3] Baboolal, S., Bharuthram, R., Two-scale numerical solution of the electromagnetic two-fluid plasma-Maxwell equations: Shock and soliton simulation. Math. and Comp. in Simulation, Vol. 76, 3-7 (2007)
[4] Barth, T.J., Numerical methods for gas-dynamics systems on unstructured meshes. In An Introduction to Recent Developments in Theory and Numerics of Conservation Laws. Lecture Notes in Computational Science and Engineering volume 5, Springer, Berlin. Eds: D. Krner, M. Ohlberger, and Rohde, C., 195-285 (1999)
[5] Dafermos, C. M., Hyperbolic conservation laws in continuum physics. Springer-Verlag, 3rd-edition (2009)
[6] Fjordholm U. S., Mishra S., Tadmor, E., Arbitrarily High order accurate entropy stable essentially non-oscillatory schemes for system of conservation laws. Preprint (2011)
[7] Gottlieb, S., Shu, C. W., Tadmor, E., Strong stability-preserving high-order time discretization methods. SIAM Rev., Vol. 43, 89-112 (2001)
[8] Goedbloed, H., Poedts, S., Principles of Magnetohydrodynamics. Cambridge University Press, 2004
[9] Hakim, A., Loverich, J., Shumlak, U., A high-resolution wave-propagation scheme for ideal two-fluid plasma equations. J. Comp. phys., Vol. 219, 418-442 (2006)
[10] Ismail, F., Roe, P. L., Affordable, entropy-consistent Euler flux functions II: Entropy production at shocks. J. Comp. Phys. Vol. 228, 5410-5436 (2009)
[11] Johnson, E.A., Rossmanith, J.A., Collisionless Magnetic Reconnection in a Five-Moment Two-Fluid Electron-Positron Plasma. Proceedings of Symposia in Applied Mathematics (proceedings of HYP2008), Volume 67.2, (2009)
[12] LeVeque, R. J., Finite Volume Methods For Hyperbolic Problems. Cambridge University Press, Cambridge (2002)
[13] Loverich, J.,Hakim, A., Shumlak, U., A discontinuous Galerkin method for ideal two-fluid plasma equations. Arxiv preprint, arXiv:1003.4542, (2010)
[14] Munz, C. D., Omnes, P., Schneider R., Sonnendru ker, E., Voβ, U. Divergence correction techniques for Maxwell solvers based on a hyperbolic model. J. Comp. Phys. Vol. 161, 484-511 (2000)
[15] Shumlak, U., Loverich, J., Approximate Riemann solvers for the two-fluid plasma model. J. Comp. Phys. 187, 620-638 (2003)
[16] Shu, C. W., TVD time discretizations. SIAM J. Math. Anal., Vol. 14, 1073-1084 (1988)
[17] Tadmor, E., The numerical viscosity of entropy stable schemes for systems of conservation laws. I. Math. Comp., Vol. 49, 91-103 (1987).
[18] Tadmor, E., Entropy stability theory for difference approximations of nonlinear conservation laws and related time-dependent problems. Act. Numerica, 451-512 (2004).

(Harish Kumar)
Seminar for Applied Mathematics (SAM)
Department of Mathematics, ETH Zürich,
Zürich, Switzerland
E-mail address: harish@math.ethz.ch

(Siddhartha Mishra)
Seminar for Applied Mathematics (SAM)
Department of Mathematics, ETH Zürich,
Zürich, Switzerland
E-mail address: siddhartha.mishra@sam.math.ethz.ch

Research Reports

No.	Authors/Title
11-22	*H. Kumar and S. Mishra* Entropy stable numerical schemes for two-fluid MHD equations
11-21	*H. Heumann, R. Hiptmair, K. Li and J. Xu* Semi-Lagrangian methods for advection of differential forms
11-20	*A. Moiola* Plane wave approximation in linear elasticity
11-19	*C.J. Gittelson* Uniformly convergent adaptive methods for parametric operator equations
11-18	*E. Kokiopoulou, D. Kressner, M. Zervos and N. Paragios* Optimal similarity registration of volumetric images
11-17	*D. Marazzina, O. Reichmann and Ch. Schwab* *hp*-DGFEM for Kolmogorov-Fokker-Planck equations of multivariate Lévy processes
11-16	*Ch. Schwab and A.M. Stuart* Sparse deterministic approximation of Bayesian inverse problems
11-15	*A. Barth and A. Lang* Almost sure convergence of a Galerkin–Milstein approximation for stochastic partial differential equations
11-14	*X. Claeys* A single trace integral formulation of the second kind for acoustic scattering
11-13	*W.-J. Beyn, C. Effenberger and D. Kressner* Continuation of eigenvalues and invariant pairs for parameterized nonlinear eigenvalue problems
11-12	*C.J. Gittelson* Adaptive stochastic Galerkin methods: beyond the elliptic case
11-11	*C.J. Gittelson* An adaptive stochastic Galerkin method
11-10	*C.J. Gittelson* Stochastic Galerkin approximation of operator equations with infinite dimensional noise